

## Experimental study of criticality in the metamagnet $\text{CsCoCl}_3 \cdot 2\text{D}_2\text{O}$

A. L. M. Bongaarts and W. J. M. de Jonge

*Department of Physics, Eindhoven University of Technology, Eindhoven, The Netherlands  
and Reactor Centrum Nederland, Petten (N.-H.), The Netherlands*

(Received 23 November 1976)

This paper reports the results of a neutron-diffraction study on the critical behavior of the induced magnetization  $M$  and the staggered magnetization  $M_{st}$  along the metamagnetic phase transition in  $\text{CsCoCl}_3 \cdot 2\text{D}_2\text{O}$ . This phase transition contains a tricritical point (TCP) at  $T_t = 1.85$  K and  $H_t = 2.70$  kOe. Critical exponents and amplitudes are obtained in the critical region  $(\alpha, \beta)$  and at the TCP  $(\alpha_t, \beta_t, \beta_1, \beta_u, \phi)$ . It is shown that the critical behavior along the critical line is in agreement with three-dimensional Ising behavior up to the TCP. In the vicinity of the TCP, crossover is observed. The tricritical behavior cannot be characterized by classical exponents. The validity of the exponents is tested by an analysis of the various tricritical scaling functions.

### I. INTRODUCTION

In recent years a fair amount of effort has been devoted to the verification of the interesting predictions of the generalized-homogeneous-function approach for phase transitions. The predictions relate to the shape of the phase boundaries and the singular behavior of thermodynamic variables as a function of the appropriate fields. They can be thought to be comprised in the hypotheses of scaling,<sup>1</sup> smoothness,<sup>2</sup> and universality.<sup>3</sup> These hypotheses assert that greatly different systems should exhibit the same general type of critical behavior.

Many of the predictions concerning ordinary critical points have been worn-out by experiments.<sup>4</sup> Particularly interesting effects occur when two or more types of order compete, giving rise to what is called multicritical points. Among those are the tricritical points (TCP), where three critical lines, bordering three coexistence phases, intersect. Points of this type can be found in  $^3\text{He}$ - $^4\text{He}$  mixtures,<sup>5</sup> in multicomponent fluid<sup>6</sup> mixtures, ferroelectrics,<sup>7</sup> structural phase transitions,<sup>8</sup> and, quite commonly, in anisotropic antiferromagnets (metamagnets).<sup>9</sup>

However, the experimental accessibility of the relevant variables is rather poor in the majority of the examples listed above. So far only a limited number of experiments have been reported and although a general consistency with the theoretical predictions can be observed it is by no means conclusive.<sup>9,10</sup>

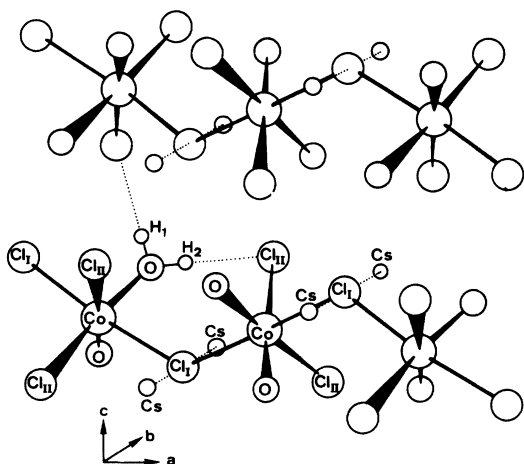
In this paper we will report our measurements on the critical behavior of the induced magnetization  $M$  and staggered magnetization  $M_{st}$  along the metamagnetic phase transition of  $\text{CsCoCl}_3 \cdot 2\text{D}_2\text{O}$ . The data are taken along the first-order triple line, at the tricritical point, and along the critical line.

Although some of the critical exponents we will report are restricted in their accuracy due to experimental limitations, we will be able to present a rather complete set of critical exponents. This paper is an extension of a Letter, published recently, in which we reported the observation of crossover near the TCP in the same system.<sup>11</sup> The organization of this paper is as follows. In Sec. II we will briefly review the existing data on  $\text{CsCoCl}_3 \cdot 2\text{H}_2\text{O}$ . Section III will be devoted to the determination of the critical exponents. In Sec. IV tricritical scaling functions will be derived and tested. The results will be summarized in Sec. V. The demagnetization corrections are treated in the Appendix.

### II. CRYSTALLOGRAPHIC AND MAGNETIC PROPERTIES

$\text{CsCoCl}_3 \cdot 2\text{H}_2\text{O}$  belongs to a series of isomorphic transitions-metal halogenides, with the structural formula  $AML_3 \cdot 2\text{H}_2\text{O}$  in which  $A = \text{Rb, Cs}$ ;  $M = \text{Mn, Fe, Co}$ ; and  $L = \text{Br, Cl}$ . All the members of this series studied so far showed pronounced linear-chain ( $d = 1$ ) characteristics.<sup>12</sup> The ratio of the interchain and intrachain exchange constants amounts to  $10^{-2}$ – $10^{-3}$ . The weak interchain couplings give rise to a three-dimensional ordered state at relatively low temperatures. The best known compound from this series is undoubtedly  $\text{CsMnCl}_3 \cdot 2\text{H}_2\text{O}$  which, together with  $(\text{CH}_3)_4\text{NMnCl}_3$  (TMMC), can be considered as one of the best physical realizations of the  $S = \frac{5}{2}$  linear-chain Heisenberg model.<sup>13</sup>

The substitution of  $\text{Mn}^{2+}$  by  $\text{Co}^{2+}$  generally results in the introduction of a large anisotropy in the exchange, since the unperturbed ground state of the  $\text{Co}^{2+}$  ion is  $3d^6$  and hence spin-orbit coupling and crystal-field effects have a drastic influence. Therefore, one may expect that the low-temperature magnetic properties of  $\text{CsCoCl}_3 \cdot 2\text{H}_2\text{O}$  will

FIG. 1. Structure of  $\text{CsCoCl}_3 \cdot 2\text{H}_2\text{O}$ .

resemble those of the Ising  $S = \frac{1}{2}$  linear chain. In this section, we will briefly review the existing experimental evidence on the behavior of the system in zero field as well as in external fields.

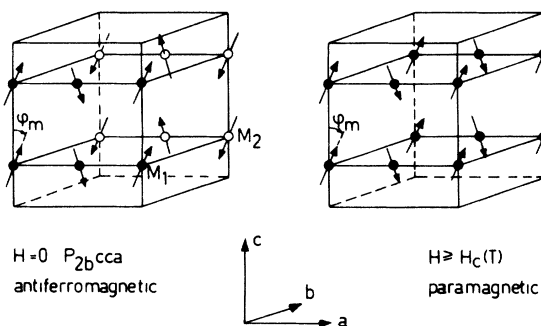
The room-temperature crystallographic structure has been determined by Thorup and Soling<sup>14</sup> as  $Pcca$  with  $a = 8.914 \text{ \AA}$ ,  $b = 7.1174 \text{ \AA}$ , and  $c = 11.360 \text{ \AA}$ . The chemical cell contains four formula units. The  $\text{Co}^{++}$  ion is surrounded by a distorted *cis*-octahedron of four chlorine and two oxygen ions. Neighboring octahedra in the  $a$  direction share one chlorine ion, thus forming chains along the  $a$  axis. The chains are separated in the  $b$  direction by layers of Cs atoms, and in the  $c$  direction by layers of hydrogen atoms (Fig. 1).

The zero-field magnetic structure of the three-dimensional antiferromagnetic state below  $T_N = 3.40 \text{ K}$  has been reported by de Jonge *et al.*<sup>15</sup> From the symmetry and magnitude of the local fields at the Cs and hydrogen positions, determined with NMR, it could be concluded that the spin arrangement can be described as a noncollinear four-sublattice array with the moments slightly canted ( $\varphi_m \approx \mp 10$ ) from the  $c$  axis in the  $a$ - $c$  plane. The magnetic space group was reported to be  $P_{2_1}cca'$ .

These results were confirmed by subsequent neutron-diffraction experiments, by Bongaarts *et al.*<sup>16</sup> The arrangement of magnetic moments is shown in Fig. 2. Due to the canting angle  $\varphi_m$ , the basically antiferromagnetic chains possess a moment in the  $a$  direction proportional to  $\sin\varphi_m$ . The chains are coupled ferromagnetically along  $c$ , and antiferromagnetically along the  $b$  direction.

#### A. Magnetic phase diagram

When a magnetic field is applied along the  $a$  direction, the system undergoes a magnetic phase

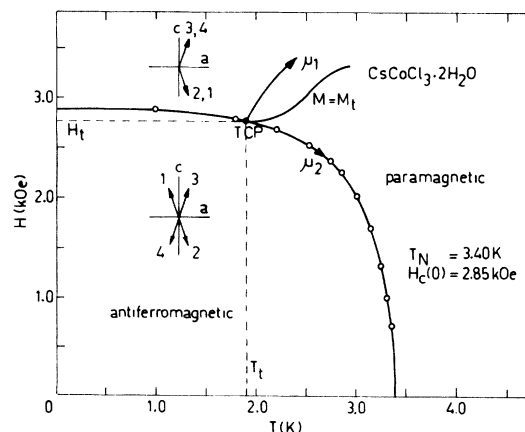
FIG. 2. Arrangement of the magnetic moments below and above the critical field  $H_c(T)$ . The moments are situated in the  $ac$  plane.

transition at  $2.85 \text{ kOe}$  at  $T = 0 \text{ K}$ . The nature of this phase transition was studied by means of NMR,<sup>17</sup> magnetization,<sup>17</sup> and neutron diffraction.<sup>18</sup> It was found that at the phase transition, the external field is sufficient to overcome the antiferromagnetic coupling of the chains in the  $b$  direction, thus giving rise to a canted two-sublattice array in the high fields (Figs. 2 and 3). When the external field is rotated either in the  $a$ - $c$  or  $a$ - $b$  plane the transition takes place when the field component in the  $a$  direction exceeds  $H_c(T)$ .

#### B. Exchange interactions

We will adopt the Hamiltonian

$$H = -2J_a \sum_a \vec{S}_i \cdot \vec{S}_{i+1} - 2J_b \sum_b \vec{S}_i \cdot \vec{S}_{i+1} - 2J_c \sum_c \vec{S}_i \cdot \vec{S}_{i+1} \quad (1)$$

FIG. 3. Magnetic phase diagram of  $\text{CsCoCl}_3 \cdot 2\text{H}_2\text{O}$  as determined by nuclear magnetic resonance. The magnetic field is applied along the  $\vec{a}$  direction. The curve  $M = M_t$  is introduced in (11).

for the system. Values for the exchange interactions obtained from specific heat, susceptibility, magnetization, afmr, and neutron diffraction have been reported. Although these results indicate a  $d=1$  Ising behavior, the actual values obtained for the exchange interactions were not quite consistent.<sup>16,17</sup>

Measurements of the specific heat by Herweyer *et al.*<sup>17</sup> and Kopinga *et al.*<sup>18</sup> showed that approximately 14% of the total magnetic entropy for a  $S=\frac{1}{2}$  system was removed below  $T_N$ . This low value for the critical entropy, comparable to the best known one-dimensional systems, warrants an interpretation of the high-temperature data on the basis of a purely one-dimensional model. Such an analysis was performed explicitly by Kopinga.<sup>18</sup> The best result was obtained assuming an Ising interaction with  $J_a/k = -38.6$  K. In the interpretation use has been made of the estimate for the lattice contribution obtained in the earlier investigations on the isomorphous Heisenberg system  $\text{CsMnCl}_3 \cdot 2\text{H}_2\text{O}$ . The value for the intrachain interaction compares very well with the earlier estimates by Herweyer *et al.* obtained from the specific heat. The value obtained from the spin-cluster-resonance<sup>17</sup> data has to be mistrusted because the use of the simplified Ising model in this case can give rise to large errors<sup>19</sup> as already quoted by Herweyer *et al.*<sup>17</sup> The antiferromagnetic interchain interaction  $J_b/k$  can be determined from the critical field at  $T=0$  K as  $J_b/k = -0.1$  K. The magnitude of the exchange constant  $J_c/k$  can be estimated by using the location of the TCP in the magnetic phase diagram which is determined by the ratio of the ferromagnetic and antiferromagnetic exchange interactions which play a role in the phase transition (Fig. 3).

As we will see later on, the TCP in  $\text{CsCoCl}_3 \cdot 2\text{D}_2\text{O}$  ( $T_N = 3.30$  K) is located at  $T_t = 1.85$  K. Using the mean-field prediction,<sup>20</sup> which in this case can be written

$$T_t/T_N = 1 - |J_b|/3J_c; \quad (2)$$

we find  $J_c/k = +0.08$  K. Application of the theory by Nagle and Bonner<sup>21</sup> gives a somewhat higher value of  $J_c/k = 0.3$  K. Application of Oguchi's formula,<sup>22</sup> inserting  $T_N = 3.30$  K gives  $|J_b/k| = |J_c/k| = 0.12$  K. Concluding, we quote  $J_a/k = -39$  K, and  $(|J_b| + |J_c|)/|J_a| \approx 8 \times 10^{-3}$ , indicating that  $\text{CsCoCl}_3 \cdot 2\text{H}_2\text{O}$  has about the same degree of one dimensionality as the isomorphous  $\text{CsMnCl}_3 \cdot 2\text{H}_2\text{O}$ .

### III. EXPERIMENTAL

The neutron-diffraction experiments that will be discussed in this paper were taken at a conventional two-crystal diffractometer at the Reac-

tor Centre, Petten. The samples were grown by evaporation of a solution containing  $\text{CsCl}$  and  $\text{CoCl}_2$  in  $\text{D}_2\text{O}$  in a molecular ratio of 1:5. The single crystals obtained this way had typical dimensions of  $5 \times 5 \times 0.5$  mm in, respectively,  $a$ ,  $b$ , and  $c$  directions.

Measurements were performed on the  $(0\frac{1}{2}0)$ ,  $(100)$ , and  $(2\frac{1}{2}0)$  superlattice reflections. The intensities  $I$  of these reflections are related to the magnetic moments, through

$$\begin{aligned} I(0\frac{1}{2}0) &\sim (M_1^a - M_2^a)^2, \\ I(1\frac{1}{2}0) &\sim (M_1^c - M_2^c)^2, \\ I(100) &\sim (M_1^c + M_2^c)^2, \\ I(2\frac{1}{2}0) &\sim (M_1^a - M_2^a)^2, \end{aligned} \quad (3)$$

where  $M_1^\alpha$  and  $M_2^\alpha$  refer to the  $\alpha$  components of neighboring spins in the  $b$  direction (Fig. 2). A comparison of the field dependence of the vicinity of the  $(1\frac{1}{2}0)$  and  $(2\frac{1}{2}0)$  reflections ensured that no traceable moment rotation occurred.<sup>16</sup> This observation leads to the conclusion that  $I(100)$  can be used for monitoring the magnetization and  $I(1\frac{1}{2}0)$  is related to the sublattice magnetization. Furthermore,  $\vec{M}_1$  and  $\vec{M}_2$  can be determined through (3).

In Sec. III, we will subsequently report on the behavior of  $M_{\text{st}}$  near  $T_N$  in zero field, the singular behavior of both  $M$  and  $M_{\text{st}}$  at the critical line, the singular behavior of  $\Delta M$  and  $\Delta M_{\text{st}}$  along the triple line, and the experimental determination of the TCP and the crossover exponent. In doing so we will assume that the critical behavior of the singular part of any thermodynamic function  $B$  can be expressed in a simple power law with exponent  $a$ . In Table I, the critical exponents and their definition as used in this paper are tabulated. These definitions follow the proposals by Griffiths,<sup>24</sup> supplemented, if necessary, by those of Riedel.<sup>25</sup>

#### A. Zero-field staggered magnetization

The temperature dependence of the order parameter  $M_{\text{st}}$  in zero field was determined by scattering experiments in the reciprocal  $a^*b^*$  plane. In order to facilitate the correction for critical scattering in the vicinity of  $T_N$ , the intensity of the  $(0\frac{1}{2}0)$  and  $(1\frac{1}{2}0)$  magnetic reflections was obtained by scanning through the corresponding reciprocal-lattice points in directions parallel and perpendicular to the  $a^*$  axis.

At temperatures  $T < 3.0$  K, the observed scattering profiles were analyzed by fitting them to a Gaussian, and adjusting the amplitude, the half-width, the position, and the background.

In the temperature region  $3.0 \leq T \leq 3.3$  K, the observed profiles of the scans parallel  $a^*$  were

TABLE I. Definition of critical exponents for a meta-magnet in the  $H_{st}=0$  plane near the critical line  $H=H_c(T)$  or  $T=T_c(H)$ .

1. Critical region:	$\left  \frac{\mu_1}{\mu_2^2} \right  \ll 1$
$M_{st}(H, T) \sim \epsilon(H, T)^\beta$	$H \leq H_c(T)$
$\chi_{st}(H, T) \sim \epsilon(H, T)^{-\gamma'}$	$H \leq H_c(T)$
$C_H(T) \sim (T_c - T)^{-\alpha'}$	$T \leq T_c(H)$
$\chi_T(H) \sim (H_c - H)^{-\alpha'}$	$H \leq H_c(T)$
2. Multicritical region:	$\left  \frac{\mu_1}{\mu_2^2} \right  \gg 1$
$M_{st}(\mu_1) \sim \mu_1^{\beta_t}$	$H \leq H_t$
$\chi_{st}(\mu_1) \sim \mu_1^{-\gamma_t}$	$H \leq H_t$
$C_H(T) \sim (T_t - T)^{-\alpha_t}$	$H = H_t, T < T_t$
$M_t - M \sim (H_t - H)^{1/\delta_t}$	$H \leq H_t, T = T_t$
$\chi_T(H) \sim (H_t - H)^{-\alpha_t}$	$H \leq H_t, T = T_t$
$\chi(T) \sim (T - T_t)^{-\gamma_t}$	$T \geq T_t, M = M_t$
3. First order region:	$\left  \frac{\mu_1}{\mu_2^2} \right  \ll 1$
$\Delta M_{st} \sim \mu_2^{\beta_1}$	$\mu_1 = 0$
$\Delta M \sim \mu_2^{\beta_u}$	$\mu_1 = 0$
$M^* - M_t \sim \mu_2^{\beta^+}$	$\mu_1 = 0$
$M_t - M^- \sim \mu_2^{\beta^-}$	$\mu_1 = 0$

corrected for critical scattering. This was not necessary for the scans perpendicular  $a^*$ . The critical scattering manifests itself in this scan direction as an increased background, which was a free parameter in the least-squares analysis.

The intensities of the  $(0\frac{1}{2}0)$  reflection were corrected for the nuclear contribution originating from the second-order wavelength contamination. From measurements for  $T > T_N$  this temperature-independent contribution was found to be 6% of the total intensity of the  $(0\frac{1}{2}0)$  reflection at  $T = 1.2$  K. In the temperature region  $3.0 < T < 3.3$  K, the critical scattering in the vicinity of the  $(0\frac{1}{2}0)$  reciprocal-lattice point showed the same planar shape. Therefore, only the scans parallel  $a^*$  could be used for the determination of the long-range order in this temperature region.

The temperature dependence of  $M^a$  and  $M^c$  as obtained from the square root of the intensity of the  $(0\frac{1}{2}0)$  and  $(1\frac{1}{2}0)$  Bragg reflections, reduced to 1 at  $T=0$ , is given in Fig. 4 as a function of reduced temperature  $T/T_N$  together with the NMR data.<sup>17</sup> It is seen that, within the experimental accuracy,  $M^a$  and  $M^c$  can be scaled on each other. This implies that the canting angle  $\varphi_m$ , see Fig. 2,

is essentially temperature independent.

In order to be able to compare the results of  $\text{CsCoCl}_3 \cdot 2\text{D}_2\text{O}$  with various theoretical models, we have included in Fig. 4 the predictions of the mean-field, and the  $d=2$  and  $d=3$  Ising model for a simple cubic (sc) lattice with  $S = \frac{1}{2}$ .<sup>23</sup> From Fig. 4 it may be seen that the  $d=3$  Ising model gives the best description of the temperature dependence of the order parameter in  $\text{CsCoCl}_3 \cdot 2\text{D}_2\text{O}$ . In the vicinity of the critical point the decrease of the order parameter is described by (see Table I):

$$M_{st}(T)/M_{st}(0) = B_T(1 - T/T_N)^{\beta_T}.$$

The data in the temperature region  $3.0 < T < 3.30$  K were fitted to this power law by a least-square analysis, in which each data point was weighted inversely proportional to its estimated error. Including data corresponding to temperature  $T \leq 3.0$  K decreased the quality of the fit, indicating the breakdown of the power-law behavior away from  $T_N$ .

The results for the best fit, with all parameters allowed to vary freely is shown in Fig. 5. The corresponding final values for the parameters and the 90% confidence limits are

$$\begin{aligned} T_N &= 3.30 \pm 0.01 \text{ K}, \\ B_T &= 1.55 \pm 0.05 \text{ K}, \\ \beta_T &= 0.298 \pm 0.006 \text{ K}. \end{aligned} \quad (4)$$

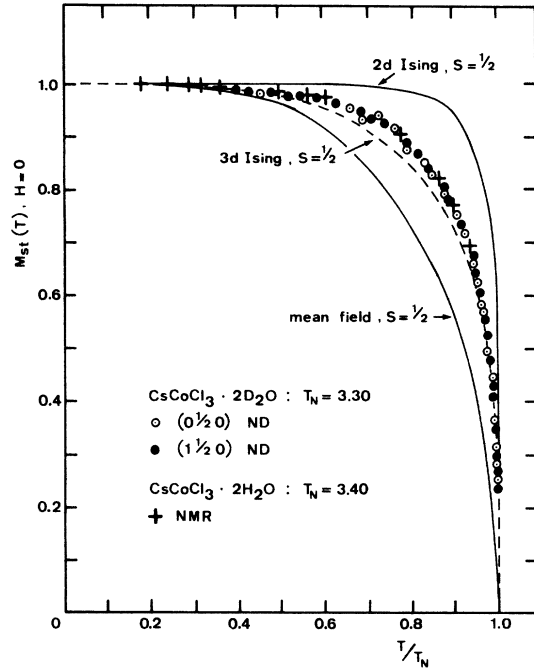


FIG. 4. Reduced temperature dependence of the zero-field staggered magnetization of  $\text{CsCoCl}_3 \cdot 2\text{D}_2\text{O}$ ,  $T_N = 3.40$  K, and  $\text{CsCoCl}_3 \cdot 2\text{H}_2\text{O}$ ,  $T_N = 3.30$  K, as determined by NMR and neutron diffraction.

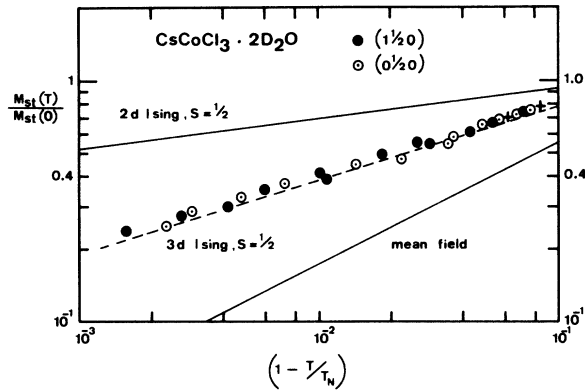


FIG. 5. Double-logarithmic plot of the temperature dependence of the reduced zero-field staggered magnetization of  $\text{CsCoCl}_3 \cdot 2\text{D}_2\text{O}$  in the critical region.

These values of  $B_T$  and  $\beta_T$  differ from those reported earlier<sup>16</sup> due to a different analysis of the critical scattering.

#### B. Critical line, $T_t < T < T_N$

Figure 6 shows a typical example of the behavior of  $M_1$ ,  $M_2$ ,  $M$ , and  $M_{st}$  as a function of magnetic field in the critical region. The data are corrected for demagnetizing effects according to the procedure outlined in the Appendix.

The order parameter  $M_{st} \equiv \bar{M}_1 - \bar{M}_2$  decreases to zero when the critical line is passed, whereas  $M \equiv \bar{M}_1 + \bar{M}_2$ , remains smooth as may be expected for a nonordering density. The essentially different nature of these two thermodynamic densities is also indicated by the observation of critical scattering in the vicinity of the  $(1\frac{1}{2}0)$  reflection whereas the critical scattering around the  $(100)$  reflection could hardly be detected. The critical scattering around  $(1\frac{1}{2}0)$  is a function of  $H$ , peaks at the phase boundary, and showed the same planar shape, characteristic for the fluctuations in  $d=1$  systems, as found in zero field near  $T_N$ .

The critical behavior of  $M$  and  $M_{st}$  is expressed by

$$M_{st} \approx [1 - H/H_c(T)]^\beta, \quad (5)$$

$$|M - M_c(T)| \approx |1 - H/H_c(T)|^{1-\alpha}.$$

In a former paper,<sup>11</sup> we reported that both  $\alpha$  and  $\beta$  were constant ( $\alpha = 0.15$ ,  $\beta = 0.295$ ) along the critical line, thus supporting the prediction of the smoothness hypothesis. Close to the multicritical point, crossover from critical to tricritical behavior was found as illustrated in Figs. 7 and 8. The tricritical values of  $\alpha$  and  $\beta$  were found to be  $\alpha_t = 0.65$ ,  $\beta_t = 0.15$  ( $T_t = 1.85$  K,  $H_t = 2.75$  kOe). These facts were verified using the asymptotic behavior

of Riedel's crossover scaling functions<sup>25</sup> to which we will return later.

#### C. First-order phase transition $T < T_t$

For temperature below  $T = 1.85$  K the  $M_1(H_{ext})$  curves, as determined from the normalized Bragg intensities of the  $(1\frac{1}{2}0)$  and  $(100)$  reflections using (3), showed the unphysical behavior  $M_1 > 1$  in the vicinity of the phase border  $H = H_c(T)$ , indicating a first-order phase transition. Additional evidence for the different nature of the phase transition was the absence of critical scattering below  $T \approx 1.85$  K.

After correction for demagnetizing effects and removal of the rounding off  $M_{st}$ ,  $M$ ,  $M_1$ , and  $M_2$  all showed a discontinuity at the phase border.

The discontinuities of the staggered magnetization  $\Delta M_{st}$  and the induced magnetization  $\Delta M$  may both serve to define an order parameter.<sup>24</sup> These discontinuities vanish if the tricritical point is approached along the first-order line  $H = H_c(T)$  for  $T < T_t$ . This may be described by the exponents  $\beta_1$  and  $\beta_u$ , see Table I.

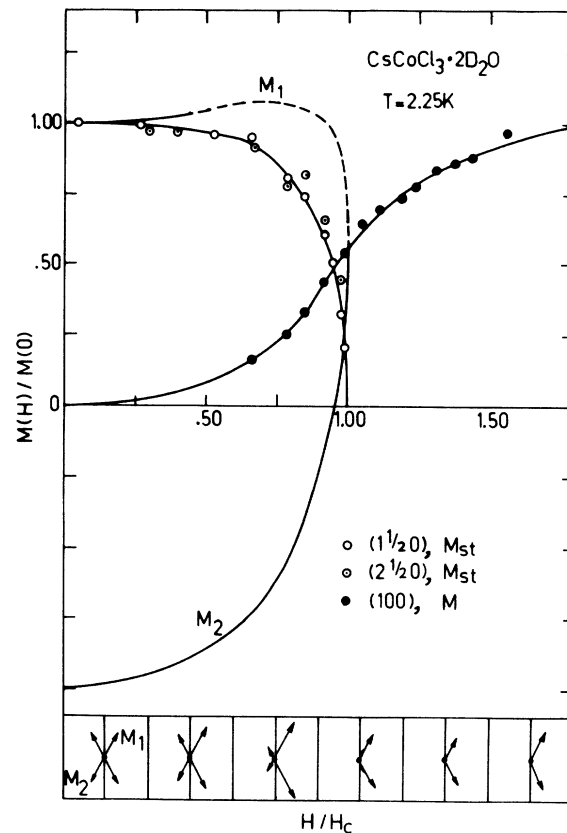


FIG. 6. Field dependence of  $M$ ,  $M_{st}$ ,  $M_1$ , and  $M_2$  for  $T > T_t$ .

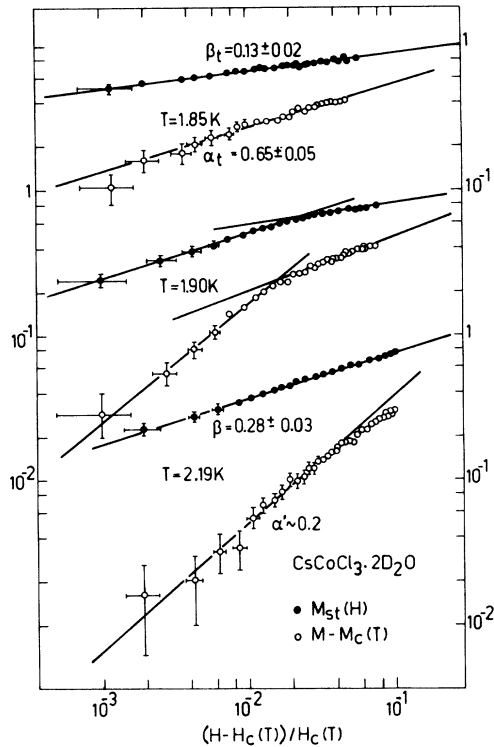


FIG. 7. Double logarithmic plot of the field dependence of the staggered magnetization and the magnetization for three different temperatures;  $T = 2.19 \text{ K}$  ordinary critical behavior,  $T = 1.90 \text{ K}$  crossover, and  $T = 1.85 \text{ K}$  tricritical behavior.

Consider first the discontinuity in the induced magnetization  $\Delta M(T)$ . At the first-order line,  $H = H_c(T)$ ,  $M(H)$  can have two values, which are called  $M^-(T)$  as the limiting value coming from the antiferromagnetic region,  $H \leq H_c(T)$ , and  $M^+(T)$  as the value corresponding to the disordered region,  $H \geq H_c(T)$ , such that

$$\Delta M(T) = M^+(T) - M^-(T). \quad (6)$$

The temperature dependence of  $M^+(T)$  and  $M^-(T)$  can be used to construct a "density-field" phase diagram, see Fig. 9. The error bars indicate the corrections made by removing the rounding off as mentioned in the Appendix.

For temperatures below  $T = 1.85 \text{ K}$ , Fig. 9 shows the mixed state in which paramagnetic and antiferromagnetic domains coexist in varying proportions depending on the demagnetization factor of the sample. For  $T > 1.85 \text{ K}$  we have included the values of  $M$  at the critical line, which is indicated with  $M_c(T)$ .

The vanishing of the discontinuities in  $\Delta M(T)$ ,  $M^+(T) - M_t$ , and  $M_t - M^-(T)$  at the TCP may be described by the exponents  $\beta_u$ ,  $\beta^+$ , and  $\beta^-$ , respectively. Scaling predicts that  $\beta^+ = \beta^- = \beta_u$ . Fig-

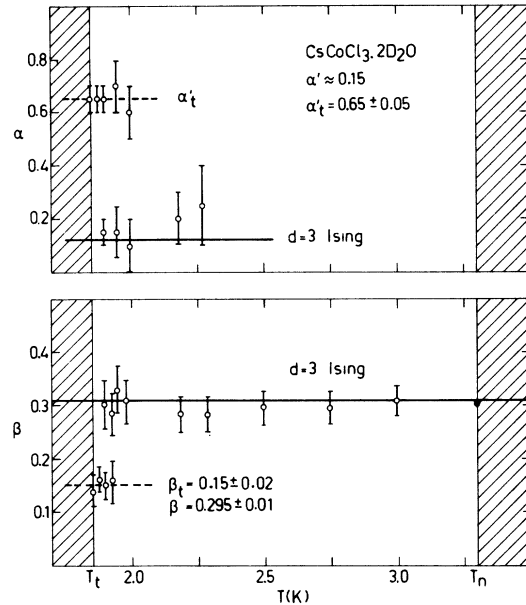


FIG. 8. Demonstration of the validity of the smoothness hypothesis in  $\text{CsCoCl}_3 \cdot 2\text{D}_2\text{O}$  for the exponents  $\alpha$  and  $\beta$  determined from isothermal scans. The full dot is the result for  $\beta$  in zero field. Drawn lines represent the prediction of the three-dimensional Ising model; dashed lines, the estimated values for the tricritical exponents.

ure 10 shows a double logarithmic plot of these entities as a function of reduced temperature. The best result was obtained with  $T_t = 1.85 \text{ K}$  and  $M_t = 0.63$ , for which we find  $\beta_u = \beta^+ = \beta^- = 0.72$ . However, the possible errors involved may be quite large and are mainly due to the corrections for rounding off, as indicated by the vertical error bars in Fig. 10. In fact, with the information of Fig. 10 alone, the TCP ( $T_t, M_t$ ) cannot be located

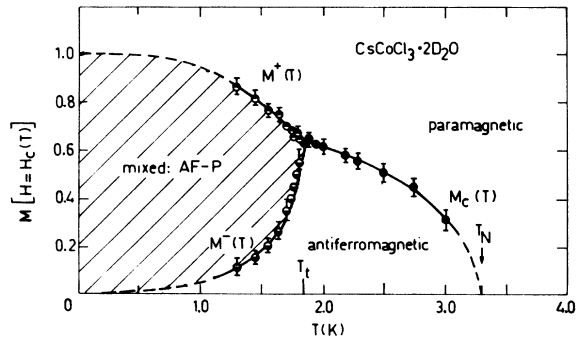


FIG. 9. Temperature dependence of the induced magnetization along the phase border  $H = H_c(T)$ . For  $T < 1.85 \text{ K}$  there is a mixed, antiferromagnetic-paramagnetic, state caused by the discontinuity in the magnetization.

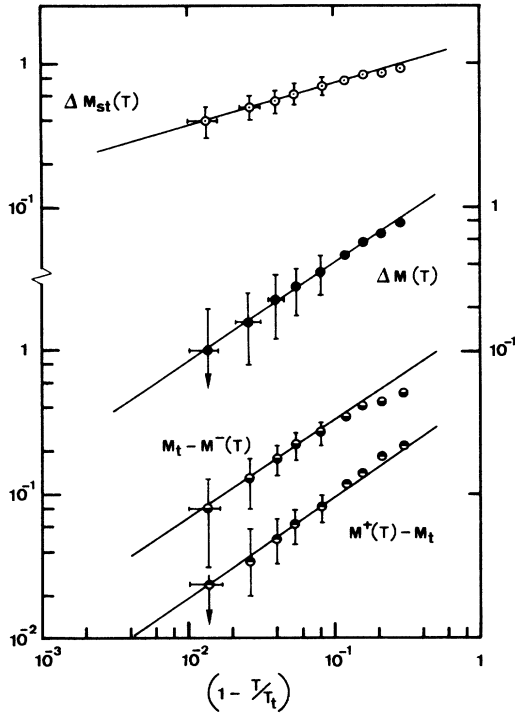


FIG. 10. Double-logarithmic plot of  $\Delta M_{st}(T)$ ,  $\Delta M(T)$ ,  $M^+(T) - M_t$ , and  $M_t - M^-(T)$  vs reduced temperature along the triple line for  $T_t = 1.85$  K and  $M_t = 0.63$ .

very precisely. Therefore we shall use a different approach, which proves to be more successful.

Consider the temperature dependence of the magnetization for  $H = H_c(T)$  in the paramagnetic region, i.e.,  $M^+(T)$  for  $T < T_t$  and  $M_c(T)$  for  $T > T_t$ . As can be seen from Fig. 9 at the point, where the  $\lambda$ -line  $M_c(T)$  and the upper phase boundary  $M^+(T)$  intersect, there is a clear difference in slope, which can be found without first applying a demagnetization correction and may serve to locate the TCP:

$$\begin{aligned} T_t &= 1.85 \pm 0.02 \text{ K}, \\ M_t &= 0.63 \pm 0.01 \text{ K}. \end{aligned} \quad (7)$$

Using these values and considering the possible systematic errors involved in the demagnetization correction, we obtain the following values for the tricritical exponents connected with the discontinuity in the induced magnetization:

$$\begin{aligned} \beta_u &= 0.7 \pm 0.3, \quad \beta^+ = 0.7 \pm 0.4, \\ \beta^- &= 0.7 \pm 0.4, \quad B_u = 2.2 \pm 0.8. \end{aligned} \quad (8)$$

The larger possible error of  $\beta^+$  and  $\beta^-$  is caused by the uncertainty of  $M_t$ . If we demand that  $\beta^+ = \beta^-$ , we obtain the same result as for  $\beta_u$ . The theoretic-

cal prediction for these exponents is  $\beta_u = \beta^+ = \beta^- = 1$ . Although the measurements strongly suggest that the exponents in  $\text{CsCoCl}_3 \cdot 2\text{D}_2\text{O}$  are smaller, the prediction of theory cannot be excluded.

The discontinuity in the staggered magnetization  $\Delta M_{st}(T)$  is presented in Fig. 11. Again, rather large errors may be involved due to the correction for the distribution in the internal field in the sample. A double logarithmic plot of  $\Delta M_{st}(T)$  versus reduced temperature was constructed in order to detect the anticipated power-law behavior

$$\Delta M_{st}(T) = B_1(1 - T/T_t)^{\beta_1}. \quad (9)$$

The best fit, shown in Fig. 10 resulted in

$$\begin{aligned} T_t &= 1.85 \pm 0.02 \text{ K}, \\ \beta_1 &= 0.30 \pm 0.15, \quad B_1 = 1.25 \pm 0.05. \end{aligned} \quad (10)$$

#### D. Crossover exponent

The crossover exponent  $\varphi$  determines the shape of the phase boundary at the TCP and relates the various sets of exponents. It can be determined independently and directly by a procedure recently suggested by Giordano.<sup>26</sup> He derived that

$$H'(T) - H_c(T) \sim P(T/T_t - 1)^\varphi. \quad (11)$$

$H'(T)$  denotes the field where the magnetization equals the magnetization at the TCP. This curve is drawn in Fig. 3. A double logarithmic plot of these data is shown in Fig. 12. As in the case of  $^3\text{He}$ - $^4\text{He}$  mixtures and dysprosium aluminum garnet tested by Giordano,<sup>26</sup> again (11) seems to be valid up until rather high temperatures. The resulting values are

$$\begin{aligned} \varphi &= 2.0 \pm 0.2, \quad T_t = 1.85 \pm 0.02 \text{ K}, \\ P &= (1.45 \pm 0.08) H_t. \end{aligned} \quad (12)$$

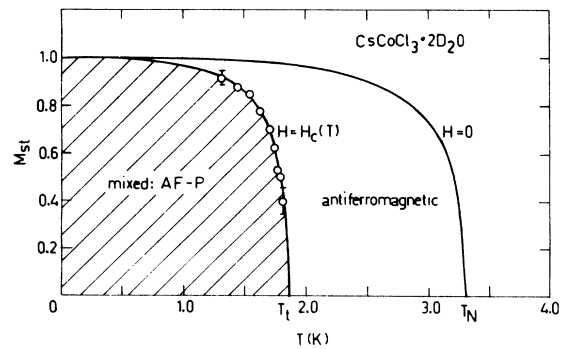


FIG. 11. Temperature dependence of the staggered magnetization for  $H = H_c(T)$  and  $H = 0$ . The full line through the data points is obtained from the zero-field data with  $T_t = 1.85$  K.

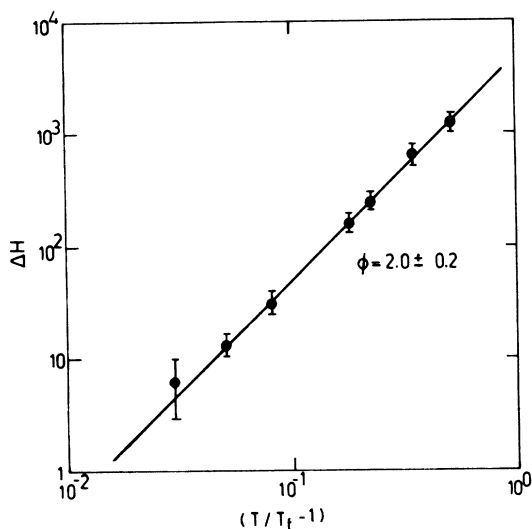


FIG. 12. Plot of  $\Delta H = H'(T) - H_c(T)$  vs temperature, yielding the crossover exponent  $\phi$ .

#### E. Tricritical point

So far we have treated the  $T_t$  or  $H_t$  as adjustable parameters in a number of fits. All the resulting values for  $T_t$  and  $H_t$  were well within the quoted statistical errors. It seems therefore that we may limit the possible error in these parameters. Moreover, independent estimates for  $T_t$  were obtained from the temperature dependence of the intersection of the  $(1\frac{1}{2}0)$  and  $(100)$  intensity versus field curves, from the temperature dependence of the induced magnetization  $M$  in the paramagnetic region (see Fig. 9,) and from the observation of crossover specifically in  $M_{st}$  near the TCP.

Therefore we feel confident that the tricritical point may be located at

$$T_t = 1.85 \pm 0.01 \text{ K}, \quad (13)$$

$$H_t = 2.70 \pm 0.05 \text{ kOe}.$$

Using these values, the statistical errors in the various exponents determined above may be reduced, which leads to the following set of indices:

$$\begin{aligned} \beta_1 &= 0.30 \pm 0.10, & \alpha_t &= 0.65 \pm 0.05, \\ \beta^+ &= 0.7 \pm 0.3, & \beta_t &= 0.15 \pm 0.02, \\ \beta^- &= 0.7 \pm 0.3, & \phi &= 2.0 \pm 0.2, \\ \beta_u &= 0.7 \pm 0.2, \end{aligned} \quad (14)$$

These exponents do satisfy the scaling relations  $\beta_1 = \phi\beta_t$  and  $\beta_u = \phi(1 - \alpha_t)$ , but are clearly not in agreement with present theoretical predictions for a tricritical point.

In Sec. IV, we will investigate the validity of the

exponents by fitting the experimental data of  $M_{st}(H, T)$ , and  $M(H, T)$  to the various ways in which the equation of state can be written at the TCP.

#### IV. TRICRITICAL SCALING FUNCTIONS

So far we have used the results obtained in isothermal scans directly. However, the applications of scaling theory provides a method of testing the consistency of the critical exponents in which the data from the entire neighborhood of the tricritical point can be used. In this way, one may also hope to eliminate the main source of inaccuracy in the individual scans close to the critical field, that is, the distribution of internal fields due to the nonperfect sample shape.

##### A. Scaling functions

Theory prescribes<sup>24,25</sup> that in the  $H_{st} = 0$  plane the scaling fields  $\mu_1$  and  $\mu_2$  should be chosen,

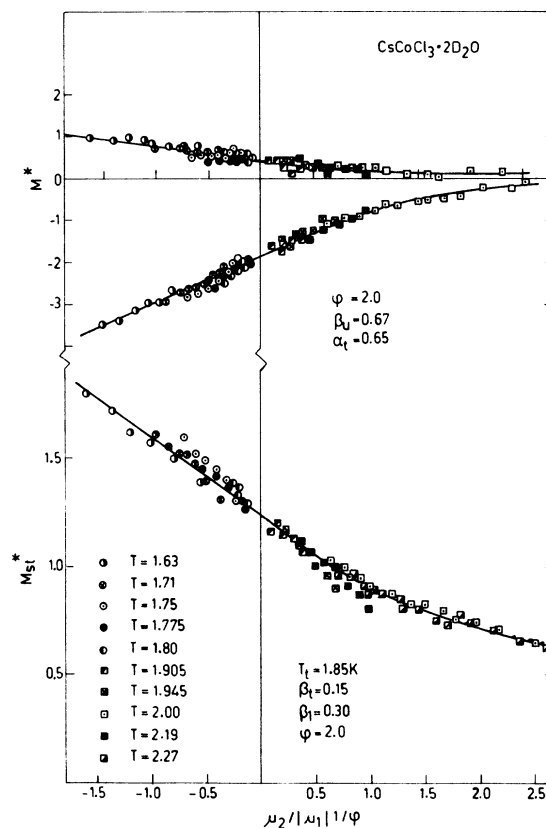


FIG. 13. Experimental data of the magnetization (upper part) and staggered magnetization (lower part) near the tricritical temperature according to Eq. (16a). The two branches for the  $M^*$  correspond to the sign of  $\mu_1$ .

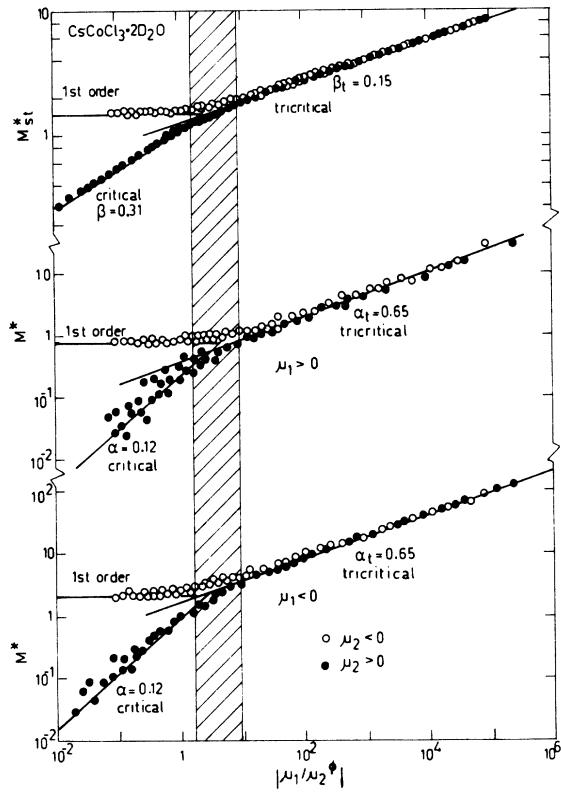


FIG. 14. Double logarithmic plot of the scaled magnetization  $M^*$  and the scaled staggered magnetization  $M_{st}^*$  according to Eq. (16b). The drawn lines represent the predicted asymptotic behavior according to Eq. (17). The shaded region indicates the 25% crossover region.

respectively, nonparallel and parallel to the phase boundary at the TCP. A convenient choice of scaling fields is

$$\mu_1 = [H - H_c(T)]/H_t, \quad (15)$$

$$\mu_2 = (T - T_t)/T_t - C\mu_1,$$

in which the coefficient  $C$  can be varied if necessary. The scaling fields are shown in Fig. 3.

From the homogeneity of the free energy asymptotically close to the TCP the following scaling functions  $B^*$  for  $B(\mu_1, \mu_2)$  with exponents  $a$  and  $a_t$  can be derived<sup>24,25</sup>:

$$B_1^*(\mu_2/\mu_1^{1/\varphi}) = B(\mu_1, \mu_2)/\mu_1^a, \quad (16a)$$

$$B_2^*(\mu_1/\mu_2^\varphi) = B(\mu_1, \mu_2)/\mu_2^{a_t}. \quad (16b)$$

The scaling functions  $B_2^*$  depends only on  $\mu_1/\mu_2^\varphi$  and is expected to show the following asymptotic behavior<sup>25</sup>:

$$\begin{aligned} B_2^* &\sim (\mu_1/\mu_2^\varphi)^a && \text{in the critical region,} \\ B_2^* &\sim (\mu_1/\mu_2^\varphi)^{a_t} && \text{in the tricritical region,} \\ B_2^* &\sim \text{const} && \text{in the first-order region.} \end{aligned} \quad (17)$$

For the scaling of the experimental data of  $\text{CsCoCl}_3 \cdot 2\text{D}_2\text{O}$ , we used the values of  $\varphi$ ,  $\alpha_t$ ,  $\beta_t$ ,  $H_c(T)$ , and  $M_t$  as obtained in the isothermal scans.

### B. Experimental

Figure 13 shows the data collapsing of the scaled data of  $M_{st}(\mu_1, \mu_2)$  and  $[M(\mu_1, \mu_2) - M_c(T)]/M_t$  as a function of  $\mu_2/\mu_1^{1/\varphi}$  [scaling function  $B_1^*(\mu_2/\mu_1)$  using the scaling fields  $\mu_1$  and  $\mu_2$  with  $C=0$ , Eq. (15)].

The scaling function  $B_2^*(\mu_1/\mu_2^\varphi)$  for  $M_{st}$  and  $M$  are shown in Fig. 14. The data are plotted on a logarithmic scale in order to detect the asymptotic behavior predicted by Riedel.<sup>25</sup> For the scaling fields we used here,  $C=1$ . Apart from the apparent data collapsing, the predicted asymptotic behavior seems to be satisfied, as shown by the straight lines in the plots. The shaded area is the crossover region which was discussed in a previous Letter.<sup>11</sup>

Finally we have studied the effect on the scaled data of a change of the inserted exponents  $\varphi$ ,  $a_t$ , and  $\beta_t$ , as well as the effect of a different choice of  $\mu_1$  and  $\mu_2$ .

For this purpose we constructed the scaling functions of the type  $B_1^*$  and  $B_2^*$  also for the classical TCP exponents  $\alpha_t = \frac{1}{2}$  and  $\beta_t = \frac{1}{4}$ . It was found that these results, in terms of data collapsing, were inferior to the ones obtained with the experimental  $\alpha_t = 0.65$  and  $\beta_t = 0.15$ . The quality could not be improved by varying the other variables  $T_t$  or  $H_t$ .

The variation of the coefficient  $C$  in the definition of  $\mu_1$  and  $\mu_2$  [Eq. (15)] was found to have no significant effect on the data collapsing in the

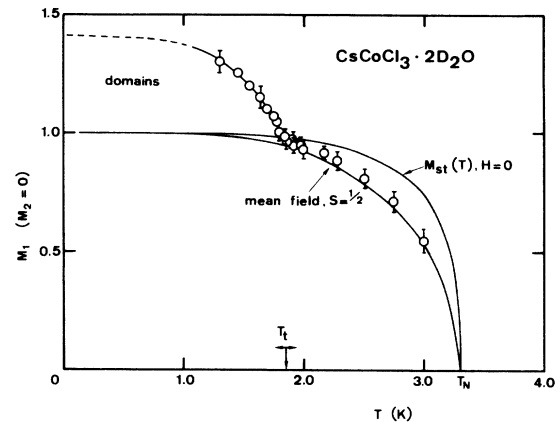


FIG. 15. Temperature dependence of  $M_1$  if  $M_2 = 0$ ;  $I_{1 \frac{1}{2}}(H, T) = I_{100}(H, T)$ . For  $T > 1.9$  K, we show that the replacement of the molecular field of a sublattice by the internal magnetic field in the sample induces mean-field behavior. For  $T < 1.8$  K, this analysis fails, indicating the presence of domains in the sample.

TABLE II. Summary of tricritical exponents in various systems.

System	$\alpha_t$	$\beta_t$	$\varphi$	$\beta_+$	$\beta_-$	$\beta_u$	$\beta_1$
CsCoCl <sub>3</sub> ·2D <sub>2</sub> O	0.65 ± 0.05	0.15 ± 0.02	2.0 ± 0.2	0.7 ± 0.3	0.7 ± 0.3	0.70 ± 0.20	0.3 ± 0.1
FeCl <sub>2</sub> (Ref. 28)	...	...	~2	1.03 ± 0.05	0.36 - 1.13	1.11 ± 0.11	0.19 ± 0.02
DyAlG (Ref. 29) {110}	...	...	1.95 ± 0.11	1	1	0.98 ± 0.05	...
<sup>3</sup> He- <sup>4</sup> He (Ref. 5)	0.5	...	2.08 ± 0.12	1	1	1 ± 0.05	...
ND <sub>4</sub> Cl (Ref. 8)	0.67	0.12	...	...	...	...	...
Theory	0.5	0.25	2	1	1	1	0.5

range studied  $0 < C < 2$ . The only effect was a changing of the width of the 25% crossover region.<sup>27</sup> For  $C=0$ , the crossover covered about two decades, as predicted by Riedel and Wegner.<sup>27</sup> For  $C=1$ , the crossover region decreased to about one decade.

Concluding this section we like to note that good data collapsing was obtained with the experimental nonclassical exponents  $\alpha_t = 0.65$ , and  $\beta_t = 0.15$ . The fact that the *same* experiment yields the *critical* exponents  $\alpha = 0.12$ , and  $\beta = 0.30$  in agreement with the expected three-dimensional Ising behavior adds further evidence to the validity of scaling near the TCP and the values of the TCP exponents.

## V. SUMMARY

In Table II we have summarized the tricritical exponents obtained in the present experiment on CsCoCl<sub>3</sub>·2D<sub>2</sub>O together with the results obtained for other systems and the theoretical predictions for a classical tricritical point. A comparison of these results is rather difficult because in the majority of systems only a restricted number of exponents is known. Except for the present case, in none of the systems are both the tricritical exponents ( $\beta_u$ ,  $\beta_1$ ,  $\beta_+$  and  $\beta_-$ ) and the exponents  $\alpha_t$ ,  $\beta_t$  measured, so that in those cases the consistency of both exponents through the scaling relations  $\beta_1 = \varphi\beta_t$  and  $\beta_u = \varphi(1 - \alpha_t)$  cannot be tested.

Among the different systems tabulated in Table II, dysprosium aluminum garnet<sup>29</sup> (DyAlG) is probably the most closely related to CsCoCl<sub>3</sub>·2D<sub>2</sub>O in the sense that in both cases we are dealing with a complicated magnetic array. It seems, however, that the newest optical data on  $\beta_+$ ,  $\beta_-$ , and  $\beta_u$  gives a good agreement with the classical prediction. Although our data is not as accurate for these exponents, the classical behavior does not seem to be satisfied.

As for the exponents  $\alpha_t$  and  $\beta_t$ , the only comparable data up till now comes from the order-disorder transition in ND<sub>4</sub>Cl. As can be seen in Table II, the agreement is astonishing, although quite inconsistent with the theoretical predictions. Garland *et al.*<sup>8</sup> suggest that in the cases of ND<sub>4</sub>Cl

the value of the exponents can be explained assuming a multicritical point of the order four. Whether the explanation of the inconsistency with the theoretical predictions in the case of CsCoCl<sub>3</sub>·2D<sub>2</sub>O must be sought in this direction remains to be seen. For the moment we feel that the existing experimental evidence is too limited to justify firm conclusions.

## ACKNOWLEDGMENTS

It is a pleasure to acknowledge the cooperation and stimulating discussions with Dr. J. Bergsma, Dr. E. Frikkee, J. A. J. Basten, Professor Dr. P. van der Leeden and Dr. K. Kopinga. One of the authors (W. J. M. de J) wishes to acknowledge a grant from the "Netherlands Organization for the Advancement of Pure Research (ZWO)." This work is partially supported by the "Stichting Fundamenteel Onderzoek der Materie (FOM)."

## APPENDIX: DEMAGNETIZATION CORRECTIONS

In general, experiments in a magnetic field give rise to demagnetizing effects which cause the internal magnetic field  $H_{\text{int}}$  in the sample to be different from the externally applied magnetic field  $H_{\text{ext}}$ ,

$$\vec{H}_{\text{int}} \equiv \vec{H}_{\text{ext}} - N \vec{M}(H_{\text{ext}}, T) . \quad (\text{A1})$$

The demagnetization factor  $N$  depends on the shape of the sample and can only be defined for quadratic surfaces.

It has been pointed out by Wyatt<sup>30</sup> that a sample with a finite demagnetization factor  $N \neq 0$  can not undergo a discontinuity in the induced magnetization  $M(H_{\text{ext}}, T)$  at a first-order phase transition. For if at  $H_{\text{int}} = H_c(T)$  the magnetization suddenly went from the antiferromagnetic value  $M^-(T)$  to the paramagnetic value  $M^+(T)$  there would be an increase in the demagnetizing field of  $N[M^+(T) - M^-(T)]$ , which would lower the field inside the sample below the critical value. Therefore, in the external field range

$$H_c(T) + NM^-(T) < H_{\text{ext}} < H_c(T) + NM^+(T) ,$$

the sample will be in mixed state with antiferromagnetic and paramagnetic domains. The sample will be partially magnetized, such that the internal magnetic field remains  $H_c(T)$ <sup>30</sup>:

$$M(H_{\text{ext}}, T) = (H_{\text{ext}} - H_c(T))/N, \text{ mixed state, } T < T_t. \quad (\text{A2})$$

Equation (A2) expresses how conventional magnetization measurements can be used to determine the demagnetization factor experimentally as the reciprocal of the slope of the magnetization versus field curves at a first-order phase transition.

The single crystal of  $\text{CsCoCl}_3 \cdot 2\text{D}_2\text{O}$  used for the field experiments was shaped to an ellipsoid with the dimensions  $6 \times 4 \times 0.5$  mm. However, given the extreme flatness of the sample, this could only be achieved approximately. From these dimensions the demagnetizing field,  $\vec{H}_{\text{ext}} - \vec{H}_{\text{int}}$ , at low temperatures in the paramagnetic state,  $H > H_c(T)$ , could only be estimated,  $\approx 100$  Oe.

Therefore, the demagnetization factor  $N$  and the distributions in internal fields caused by the imperfect ellipsoidal shape of the sample were determined experimentally.

It was found that at low temperatures the intensity versus field curves of the  $(1\frac{1}{2}0)$  and  $(100)$  magnetic reflections were rounded off. This was caused by the combined influence of a nonuniform external magnetic field across the sample and the not perfectly ellipsoidal shape of the sample. The rounding off could not be reduced by changing the angle of the magnetic field with the  $\vec{a}$  direction nor by illuminating only a part of the sample. The average demagnetizing field at low temperatures in the paramagnetic region,  $H \geq H_c(T)$ , was found to be 100 Oe.

The spread in internal fields in the sample, indicated by the rounding off, however, caused the onset of the first-order phase transition in the vicinity of the tricritical point to be very difficult to detect.

To overcome this difficulty we analyzed the data with a method capable of directly detecting the mixed state, using the fact that the intensity of the  $(1\frac{1}{2}0)$  and  $(100)$  magnetic reflections will be influenced by domains in the sample. To demonstrate this, consider Fig. 15 in which we have plotted

the temperature dependence of the magnetization of sublattice 1 determined from the intersection of the intensity versus  $H_{\text{ext}}$  curves of the  $(100)$  and  $(1\frac{1}{2}0)$  reflection. This, according to Eqs. (3), implies that  $M_2 = 0$ . Thus if  $I_{1\frac{1}{2}0}(H_{\text{ext}}, T) = I_{100}(H_{\text{ext}}, T)$  the internal magnetic field in the sample cancels the molecular field caused by sublattice 1 at sublattice 2. On the other hand, at sublattice 1 there can be no molecular field due to sublattice 2 ( $M_2 = 0$ ), but this field is replaced by the internal magnetic field in the sample. This is probably the reason why the temperature dependence of  $M_1(M_2 = 0)$  is well represented by the prediction of the mean field theory for  $T > 1.9$  K, as can be seen in Fig. 15. However, this analysis is no longer valid for  $T < 1.8$  K, where we find experimentally that  $M_1 > 1$ , which clearly is a nonsensical result. This indicates the presence of domains in the sample and directly leads to an estimate for the tricritical temperature  $T_t = 1.85 \pm 0.05$  K. The isotherms of  $M_1(H_{\text{ext}})$ , as determined by application of Eq. (3), were found to have the same unphysical behavior,  $M_1 > 1$ , in the vicinity of the phase border for temperatures  $T < 1.85$  K, thus providing a determination of the mixed state.

The final data discussed before have been corrected for demagnetizing effects by using the average demagnetization factor as determined experimentally from the extrapolated value to  $T = 0$  of the slope of the intensity versus field curves in the mixed state. For  $T < 1.85$  K, we have corrected the data for the inhomogeneities in the internal field by removing the rounding off in the vicinity of the phase border. This was done by demanding that  $M_1 = 1$  in the experimentally found mixed state, and that the induced magnetization  $M(H_{\text{ext}})$  has the linear behavior as expressed by Eq. (A2), such that the total "scattering power,"  $I_{1\frac{1}{2}0} + I_{100}$ , of the sample remained unaffected.

However, it will be clear that these corrections for rounding off can be a source of systematic errors. This was taken into account in the analysis of the data.

For  $T > 1.85$  K the influence of the distributions of internal fields in the sample was estimated by considering the data for different values of the demagnetization factor  $N$ .

<sup>1</sup>H. E. Stanley, *Introduction to Phase Transitions and Critical Phenomena* (Oxford University, New York, 1971).

<sup>2</sup>R. B. Griffiths and J. C. Wheeler, *Phys. Rev. A* **2**, 1047 (1970); R. B. Griffiths, *Proceedings of the 1970 Battelle Conference on Critical Phenomena*, edited by R. E. Mills, E. Ascher, and R. I. Jassee (McGraw-

Hill, New York, 1970).

<sup>3</sup>L. P. Kadanoff, in *Proceedings of the Varenna Summer-School on Critical Phenomena*, edited by M. S. Green (Academic, New York, 1971), R. B. Griffiths, *Phys. Rev. Lett.* **24**, 1479 (1970).

<sup>4</sup>For a review see, for instance, C. Domb and M. S. Green, *Phase Transitions and Critical Phenomena*,

- Vols. I-III (Academic, New York, 1972).
- <sup>5</sup>E. K. Riedel, H. Meyer, and P. Behringer, *J. Low Temp. Phys.* 22, 369 (1976).
- <sup>6</sup>P. H. Keyes, H. T. Weston, and W. B. Daniels, *Phys. Rev. Lett.* 31, 628 (1973).
- <sup>7</sup>P. S. Peercy, *Phys. Rev. Lett.* 35, 1581 (1975).
- <sup>8</sup>C. W. Garland, D. E. Bruins, and T. J. Greytak, *Phys. Rev. B* 12, 2759 (1975).
- <sup>9</sup>See, for instance, W. P. Wolf, Proceedings of the International Conference on Magnetism, Amsterdam, 1976 (unpublished).
- <sup>10</sup>J. F. Nagle and J. C. Bonner, *Ann. Rev. Phys. Chem.* 27, (1976).
- <sup>11</sup>A. L. M. Bongaarts and W. J. M. de Jonge, *Phys. Rev. Lett.* 37, 1007 (1976).
- <sup>12</sup>K. Kopinga, Q. A. G. van Vlimmeren, A. L. M. Bongaarts, and W. J. M. de Jonge, in Ref. 9; K. Kopinga, Ph.D. thesis (Eindhoven University of Technology, 1976) (unpublished).
- <sup>13</sup>H. Kobayashi, I. Tsujikawa, and S. A. Friedberg, *J. Low Temp. Phys.* 10, 621 (1973); W. J. M. de Jonge, K. Kopinga, and C. H. W. Swüste, *Phys. Rev. B* 14, 2137 (1976), and references therein; L. J. de Jongh and A. R. Miedema, *Adv. Phys.* 23, 1 (1974).
- <sup>14</sup>N. Thorup and H. Soling, *Acta Chem. Scand.* 23, 2933 (1969).
- <sup>15</sup>W. J. M. de Jonge, K. V. S. Rama Rao, C. H. W. Swüste, and A. C. Botterman, *Physica (Utr.)* 51, 620 (1971); W. J. M. de Jonge, A. L. M. Bongaarts, and J. A. Cowen, *AIP Conf. Proc.* 5, 441 (1971).
- <sup>16</sup>A. L. M. Bongaarts and B. van Laar, *Phys. Rev. B* 6, 2669 (1972).
- <sup>17</sup>A. Herweyer, W. J. M. de Jonge, A. C. Botterman, A. L. M. Bongaarts, and J. A. Cowen, *Phys. Rev. B* 5, 4618 (1972).
- <sup>18</sup>K. Kopinga, Ph.D. thesis (Eindhoven University of Technology, 1976) (unpublished).
- <sup>19</sup>J. B. Torrance and M. Tinkham, *Phys. Rev.* 187, 587 (1969).
- <sup>20</sup>J. M. Kincaid and E. G. D. Cohen, *Phys. Rep.* 22C, 57 (1975).
- <sup>21</sup>J. F. Nagle and J. C. Bonner, *J. Chem. Phys.* 54, 729 (1971).
- <sup>22</sup>T. Oguchi, *Phys. Rev.* 133, A1098 (1964).
- <sup>23</sup>C. Domb, *Phase Transition and Critical Phenomena III*, edited by C. Domb and M. S. Green (Academic, New York, 1973).
- <sup>24</sup>R. B. Griffiths, *Phys. Rev. B* 7, 545 (1973).
- <sup>25</sup>E. K. Riedel, *Phys. Rev. Lett.* 28, 675 (1972).
- <sup>26</sup>N. Giordano (unpublished).
- <sup>27</sup>E. K. Riedel and F. J. Wegner, *Phys. Rev. B* 9, 294 (1974).
- <sup>28</sup>R. Birgeneau, *AIP Conf. Proc.* 24, 258 (1975); J. A. Griffiths and S. E. Schnatterly, *AIP Conf. Proc.* 24, 195 (1975).
- <sup>29</sup>N. Giordano and W. P. Wolf, *Phys. Rev. Lett.* 35, 799 (1975); in Ref. 9.
- <sup>30</sup>A. F. G. Wyatt, *J. Phys. C* 1, 684 (1968).